ORIGINAL ARTICLE

Different growth response of mountain rangeland habitats to inter-annual weather fluctuations

Fabio Oriani[1,2,3] · Helge Aasen[2] · Manuel K. Schneider[1,3]

Abstract

Monitoring mountain rangelands is crucial for ensuring the sustainability of pastoral land use. In this study, we employ satellite image analysis to investigate how the seasonal growth patterns in the mountain rangeland ecosystem respond to inter-annual variations in weather conditions along the elevation profile. Our analysis covers nine key habitats in mountain rangelands surrounding the Swiss National Park, southeastern Swiss Alps from 2000 to 2800 m of elevation. Using the Normalized Difference Vegetation Index (NDVI) to track the growth pattern from 2016 to 2023 reveals that inter-annual weather fluctuations affect all habitats, leading to variations of 15–20% in the growth curve, with more significant impacts observed in the first half of the growing season. When comparing growth among habitats, wet and mesic pastures tend to exhibit greater growth compared to dry habitats within the elevation range of 2000–2400 m above sea level, while all habitats show a similar growth above 2400 m. Additionally, the presented statistical analysis at the landscape scale supports the existence of growth dynamics previously observed at the plot scale: that snow persistence influences the beginning of growth in pastures, but this effect is partially compensated by rapid growth following late snow melt. Conversely, in the second half of the season, growth is controlled by the onset of snow in autumn. These results demonstrate the potential of the joint application of earth observation and spatial statistics, not only to monitor the regional response to climate trends and variability, but also to differentiate inter-annual and inter-habitat responses of growth dynamics.

✉ Fabio Oriani
  fabio.oriani@protonmail.com

1 Forage Production and Grassland Systems, Agroscope, Reckenholzstrasse 191, 8046 Zurich, Switzerland

2 Water Protection and Substance Flows, Agroscope, Reckenholzstrasse 191, 8046 Zurich, Switzerland

3 Grazing Systems, Agroscope, Reckenholzstrasse 191, 8046 Zurich, Switzerland

Graphical abstract
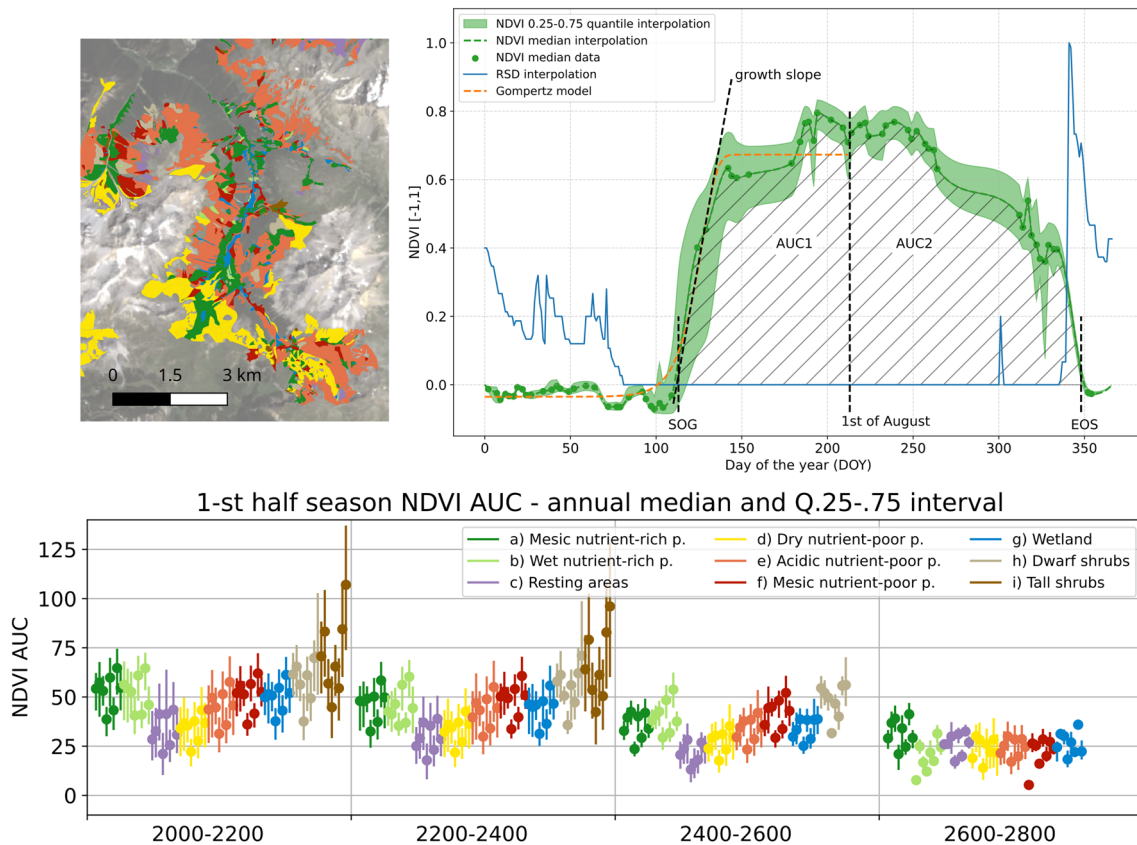
Keywords Mountain pastures · Land surface phenology · Sentinel-2 · NDVI · Climate change · Snow persistence

Introduction

Mountain rangeland vegetation covers ice- and rock-free zones on mountain ranges near the treeline. Communities of well-adapted cold-climate species have evolved to cope with harsh climatic conditions and shallow soils with limited nutrient availability (Hoersch et al. 2002; Becker et al. 2007). In the European Alps, these habitats have been grazed for millennia by domestic and wild ruminants (Schwörer et al. 2015). While change in land management by pastoralism remains the biggest change factor in alpine flora (MacDonald et al. 2000; Dirnböck et al. 2003; Cocca et al. 2012; Noroozi and Körner 2018), it is also significantly affected by variations in growth conditions (Engler et al. 2011; Du et al. 2022; Grabherr et al. 2010). In the alpine domain, the seasonal dynamics and productivity of grassland is affected by changes in temperature, water availability, and snow persistence (Ernakovich et al. 2014; Deroche et al. 2020), with variable altitudinal distribution of the species (Frei et al.

2014; Wehn et al. 2014; Inouye 2020; Crepaz et al. 2021). A comprehensive yet detailed monitoring of mountain grassland is therefore of primary importance to support pastoral management and investigate the phenology of these unique environments.

An attractive approach to monitor land surface phenology of alpine vegetation is satellite remote sensing, which regularly captures images of remote and extensive alpine areas, difficult to monitor with proximal sensing or ground survey. Because of the tendency of living vegetation to reflect near-infrared more than red light (see e.g. Wachendorf et al. 2018), the reflectance spectrum of vegetation can inform about its photosynthetic activity. In particular, the Normalized Difference Vegetation Index (NDVI), obtained from multi-band images, and other spectral indices have been used to track grassland composition and state, the seasonal growth (Taylor et al. 1985; Raab et al. 2020) and productivity (Hanna et al. 1999; Bella et al. 2004; Zhou et al. 2014; Amies et al. 2021). Other studies investigate the correlation

between NDVI and biomass (Boschetti et al. 2007; Hogrefe et al. 2017; Guerini Filho et al. 2020), or its nutritive value (Pullanagari et al. 2018; Serrano et al. 2018). Pasture spatiotemporal variations (Jin et al. 2014; Tang et al. 2023), its coverage, conversion, and degradation in time (Colpaert et al. 2003; Alves Aguiar et al. 2010; Wang et al. 2023) have also been monitored by means of spectral indices.

In mountain regions, satellite remote sensing can be applied to species-distribution mapping to detect pasture conversion (Lal et al. 1991; Boschetti et al. 2007) and monitor its management (Stumpf et al. 2020; Weber et al. 2023). Predictive classification has been recently developed to detect thematic classes linked to species richness, productivity, or topographic setting (Weber et al. 2018; Filippa et al. 2022; Huber et al. 2023). Modeling experiments analyze the pasture productivity and its degradation in relation with drought conditions (Feng et al. 2017) and to detect invasive species (Lass et al. 2005; Braunisch et al. 2016). The mentioned studies efficiently track the regional variability and change in the spatial distribution of the grassland environment.

With the present contribution, we advance this research frontier by focusing on the different local habitats composing mountain rangelands in fine-scale patterns. The so far untested driving research questions in this study are:

- Can differences in the growth season of fine-scale mountain pasture habitats be detected by satellite remote sensing?
- Which habitat types at which elevation are more sensitive to changes of inter-annual weather variability?
- How is the variability of growth different in the first part of the season from the second part?
- How are snow persistence and growth related in different habitats at a regional scale?

To answer these questions, we analyze the images provided by the satellite constellation Sentinel-2 over the rangeland surrounding the Swiss National Park, Grisons canton Switzerland, where nine habitats including dry and wet pastures, resting areas, and shrubs are mapped by field observations. Based on the spectral index NDVI, the annual variation of the growing season is analysed for each habitat. NDVI was chosen for its simplicity of computation and longtime establishment with respect to more recent vegetation indices, showing an overall similar performance with both weak and strong points. For example, well-know disadvantages of NDVI are lower saturation with dense vegetation (Asrar et al. 1984) and higher sensitivity to atmospheric and soil contamination (Huete et al. 1994). On the other hand, recent studies show that NDVI remains effective on dry vegetation detection (Zhu et al. 2024) and less sensible to topographic

influences (Matsushita et al. 2007; Ma et al. 2024) with respect to other VIs.

We derive statistical indicators from the obtained growth curves with the goal of analysing the relative changes in the vegetation growth along the elevation profile. Moreover, we analyse the impact of snow cover on different seasonal growth parameters over a period of eight years (2016–2023). This way, we characterize and compare the growth in these habitats in terms of their dependence on elevation and weather variability.

Study region and data

The Region Of Interest (ROI) of the study consists of the rangelands in the surroundings of the Swiss National Park in the Grisons canton, in an area of approximately 1000 km^2 in south-east Switzerland (Fig. 1). The region has been ground mapped for the mountain pasture habitats using the methodology by Dietl et al. (1981). The mapping involves the delineation of polygons of uniform vegetation larger than 400 m^2. To each polygon, the dominant vegetation association is attributed. In case of small-scale variability, two or three subdominant types are noted. The mountain rangelands are sparsely distributed over the ROI, with a total analyzed surface available after preprocessing ("Data preprocessing") of 15.88 km^2. We use here-on the term polygons to indicate separated areas occupied by a habitat, shown in Fig. 1 as patches of different colors according to the habitat type.

The vegetation types were aggregated to nine classes (Table 1) representing the most common rangeland habitats in the region, originating from the combination of pasture management and topographic setting. Those include nutrient-rich pastures (green shades in Fig. 1), covering a consistent portion of land along the fluvial axis of the valleys or close to buildings and roads, together with wetlands (blue color), characterized by constantly saturated soils. Distributed in higher elevation mainly above 2000 m (Table 1) are dry, acidic, and mesic nutrient-poor pastures (yellow-to-red colors in Fig. 1). They constitute the main part of the land cover, with a drier, thinner, and less fertile soil layer. In addition, high-elevation zones are populated by dwarf and tall shrubs (brown shades in Fig. 1), and by sporadic species-poor resting areas (purple color).

Within the habitats, temporal variations in the species abundance and functional properties can be due to climate (Schöb et al. 2008; Liu et al. 2018) or land-use changes (Spiegelberger et al. 2006; Mayer et al. 2009). Conversely, the habitat composition can be considered persistent in the 8-year study period, which is also strongly linked to constant topographical features. Moreover, previous research
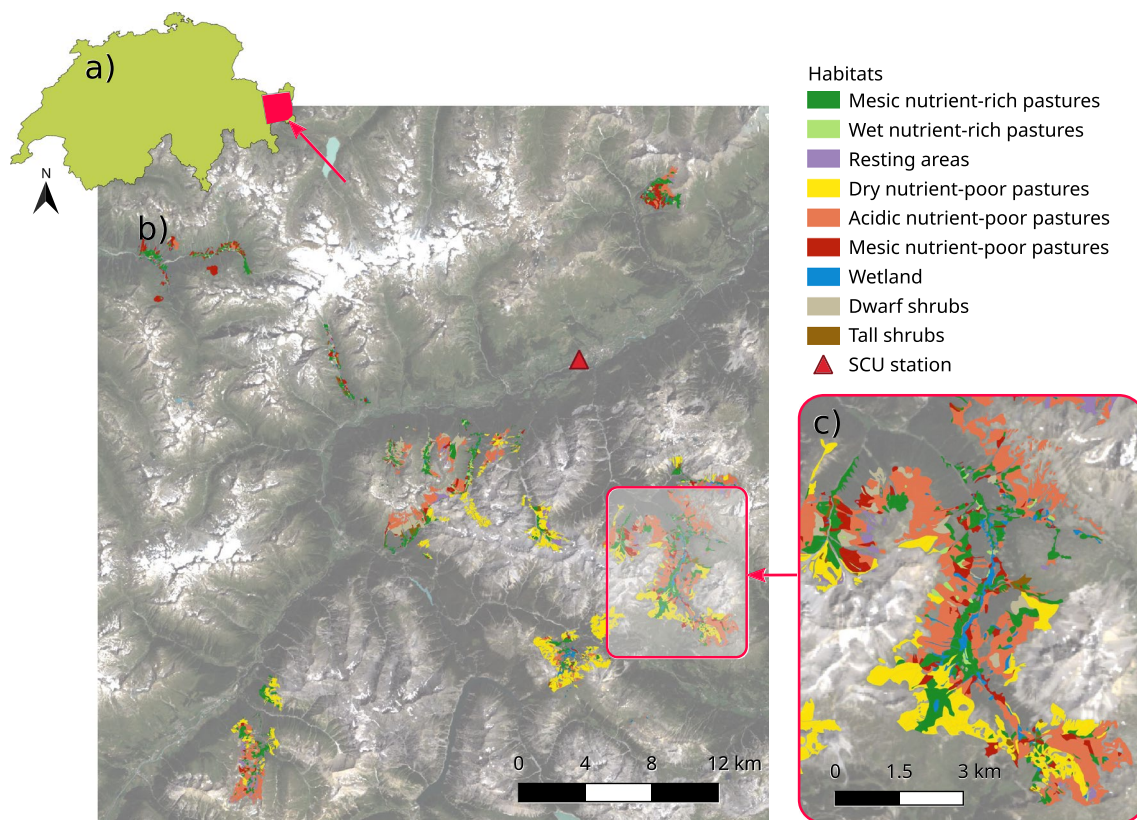
Fig. 1 Map of the study area: **a** location in Switzerland, **b** map of the mountainous region of the Swiss National Park and the mapped pasture habitats, **c** inset showing one example of the local habitat distribution

Table 1 Descriptive table of the habitats listing their total analyzed surface and the frequency distribution of the elevation values represented by its median ($Q_{0.5}$), the 0.25 ($Q_{0.25}$), and 0.75 ($Q_{0.75}$) quantiles

Analysed surface			Elevation [m]		
Habitat name	[Km²]	% of total	$Q_{0.25}$	$Q_{0.5}$	$Q_{0.75}$
Mesic nutrient-rich pastures	3.31	20.84	1769	2110	2283
Wet nutrient-rich pastures	0.19	1.20	1997	2150	2411
Resting areas	0.18	1.13	2053	2316	2528
Dry nutrient-poor pastures	2.57	16.18	2299	2371	2453
Acidic nutrient-poor pastures	5.69	35.83	2288	2419	2548
Mesic nutrient-poor pastures	2.25	14.17	1836	2159	2311
Wetland	0.51	3.21	2055	2163	2263
Dwarf shrubs	0.67	4.22	2197	2281	2367
Tall shrubs	0.51	3.21	2083	2186	2255

The surface values refer to south-ward pixels filtered by a prescribed 90°–270° aspect range (see "Annual growth curve analysis")

suggests a substantial stability of these habitats to short-term hydro-climate changes (Tang et al. 2015), with no dramatic shifts in the plant composition (Peng et al. 2017).

Ancillary variables

To analyse the elevation distribution of the habitats the digital elevation model (DEM) swissAlti3D at 2-m resolution by swisstopo (https://www.swisstopo.admin.ch/en/geodata/height/alti3d.html) was retrieved for the study region. Together with the Sentinel-2 images, the DEM was interpolated on a target grid covering the ROI with 10-m resolution (see Appendix A and Appendix B).

Moreover, to put in relation the annual growth curves with snow persistence, the daily snow depth time series was retrieved from the Scuol station (SCU) from the MeteoSwiss network (https://www.meteoswiss.admin.ch/services-and-publications/applications/measurement-values-and-measuring-networks.html#station=SCU), lying in the center of the ROI at 1304 m a.s.l. (red triangle in Fig. 1b). In this study, snow depth is not analyzed in function of elevation, but only considered at the regional scale in relation to the average start of greening (SOG) of the different habitats, to confirm the reliability of the modeled growth curves (Fig. 4). The Scuol station, with its central position in the ROI, was chosen as source of information independent from the satellite imagery for the presence of snow. Conversely, the start of greening (SOG), which

approximately coincides with snow disappearance, is spatially analysed in the study. To display the annual snow depth time series along with the annual growth curve, the relative snow depth (RDS) is computed by normalizing the values in the range [0, 1].

Methods

A workflow was developed to analyze the growth pattern of the mountain grassland habitats (for the implementation see the Code Availability section), composed of three main steps: (1) acquisition of the satellite images ("Acquisition of the satellite images"), (2) data preprocessing ("Data preprocessing"), and (3) NDVI analysis ("Annual growth curve analysis").

Acquisition of the satellite images

The satellite images from the collection Level-2A of the European Space Agency Sentinel-2 mission (https://sentinel.esa.int/web/sentinel/copernicus/sentinel-2) were used in this study. This data product offers multiband atmospherically-corrected surface reflectance images covering the visible and infrared spectrum at 10-m resolution. The subweekly revisit time of the satellite usually provides a sufficiently dense cloud-free image time series to monitor the seasonal change in mountain pastures.

All available images of the study region were acquired for the time span of 2016–2023 to analyze the seasonal growth over eight years. We used the download routine of the open-source platform EOdal (Graf et al. 2022). EOdal retrieves the images by querying the Microsoft Planetary Computer Data Catalog (https://planetarycomputer.microsoft.com/catalog) with the protocol STAC (https://stacspec.org). For the large area covered (1115 km^2), the EOdal code was adapted to run iteratively making separate queries to the data catalog and to download the images in data chunks stored locally. This also allows distributing the download process and pausing/resuming in case of server errors. In addition, preliminary data-treatment operations were applied in this phase. See the complete data acquisition workflow in Appendix A.

Data preprocessing

In order to extract the growth pattern of the pasture habitats from the NDVI time series, the acquired images were preprocessed with a novel workflow to obtain a database for pixel analysis. In the database, every pixel is associated to different attributes, including its NDVI value, habitat type, spatial grid coordinates, shadow mask, elevation, aspect, and time stamp of acquisition. The aspect as well as the shadow mask were computed based on the used DEM ("Ancillary variables").

See Appendix B for more information on the preprocessing workflow.

Annual growth curve analysis

The annual growth curves of the habitats were extracted for all available years (2016–2023) and plotted. To better isolate the growth pattern from disturbances and scatter related to the complex topography, only pixels facing southward (aspect angle between 90° and 270°) and outside the mountain shadow (shadow mask = 0) were considered. The growth curves were then generated for four classes of elevation (2000–2200, 2200–2400, 2400–2600, and 2600–2800 m respectively) to study the dependency of growth on the elevation change.

Using NDVI pixel value/date pairs extracted from the acquired annual Sentinel-2 images for every habitat, NDVI daily medians were computed to form annual curves representing the annual growth pattern. Then, a variability envelope was computed using the daily 0.25 and 0.75 quantiles (example in Fig. 2). This excluded outlier pixel data not filtered out by preprocessing, presenting mixed cover or local noise (e.g., light clouds, micro-topography shadows, isolated trees or rocks), with spectral signature non representative of the surveyed habitat. The curve values were interpolated at every day of the year (DOY) using the piece-wise interpolation Pchip (Fritsch and Butland 1984) (https://docs.scipy.org/doc/scipy/reference/generated/scipy.interpolate.pchip_interpolate.html). This technique was chosen for its stability since it preserves a smooth interpolation, but also local monotony among data points.

From the obtained growth curves, the following statistical indicators were computed to describe the growth season. The start of greening (SOG) was defined empirically as the DOY when the median growth curve goes above the prescribed threshold of 0.05 for more than five days, indicating the beginning of vegetation growth. Similarly, the end of season (EOS) occurs when the curve goes below the same threshold for five days. This fixed-threshold approach was confirmed valid by visual inspection of the curves and preferred to dynamic techniques for the detection of SOG or EOS (e.g. Fisher et al. 2006; Shang et al. 2017; Li et al. 2023). The reason for this choice is the higher robustness to scarce data and the consistency in the computation of the indicators of growth. These indicators are based on the integral of NDVI over the growth season and they are presented in the following.

The Area Under the Curve, commonly used in NDVI analysis (e.g. Weber et al. 2018; Bayle et al. 2019; Filippa et al. 2019; Yan et al. 2022) and considered as a proxy for the cumulative pattern of growth in grassland, was computed first for the first portion of the growth season (AUC1). This is delimited by the SOG and the mid-season, defined as the
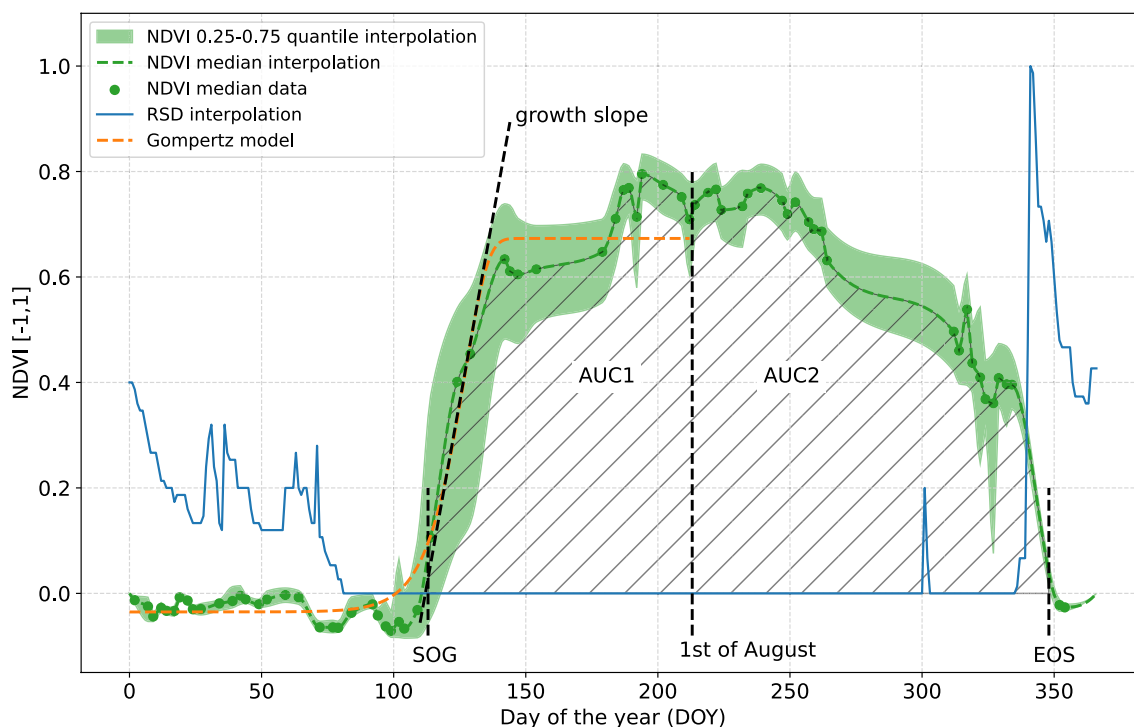
Fig. 2 Sketch of the annual curve obtained from a selected sample of NDVI data, as a function of the day of the year (DOY), with the following statistical indicators: elements in black are the derived curve indicators, namely: the start of greening (SOG) and end of season (EOS) days, the growth slope derived from the fitted Gompertz model (orange line), the areas under the curve for the first (AUC1) and second (AUC2) halves of season. The blue line indicates the relative snow depth (RSD)

1-st of August. The choice of this temporal marker is motivated by the data being generally half-away from the reach of the curve plateau to the start of the senescence (declining of the curve). It is also supported by common pastoral practice, which locates the animals in the highest and latest greening areas around this date. In addition, this choice of date as mid-season marker allows a robust and consistent comparison among habitats, being independent from the location of the growth-curve maximum or plateau, which is uncertain due to data noise and shape variability. The same indicator was computed for the second half of season (AUC2), from mid-season until the EOS, and for the whole season (AUC), from the SOG to the EOS. AUC1 and AUC2 are computed for the 0.25 and 0.75 quantile curves as well.

For both AUC1 and AUC2, statistical difference among habitats is tested separately in every elevation group using Tukey's honestly significant difference (HSD) test (Tukey 1949). The result of this test is expressed using the Compact Letter Display (CLD) method (Piepho 2004). These statistics may be affected by the uneven distribution of the data, scarcer at higher elevation. To investigate the robustness of the results to this influence factor, the same AUC analysis is repeated three times using equally sized samples of 50 pixels, which is the data amount present in the scarcest data class. These additional results are present in the supplemental material 2/2.

Moreover, the initial slope of the growth curve was modeled using the Gompertz function similarly to Schneider et al. (2006), but with a formulation adapted to the present study (see Appendix C). In particular, the used sigmoidal function (orange line in Fig. 2) defined in Eq. (1), includes the parameter c representing the ascending slope, interpreted as the growth velocity. We preferred here to use a parametric model for the growth curve only in the first part of the season, avoiding representing the senescence period with a second descending sigmoidal function. For many habitats, the NDVI values do not present a gradual decrease in autumn, with the season ending abruptly due to a major snow event, as visible in the graphs of Fig. 3. In these cases, fitting a descending sigmoidal curve was not appropriate. Moreover, modeling only the ascending part of the growth curve required a simpler equation leading to a more robust calibration, especially in case of single-polygon data (see "Comparison of seasonal indicators").

Comparison of seasonal indicators

The seasonal indicators derived from the growth curves were then compared among different habitats in four equal
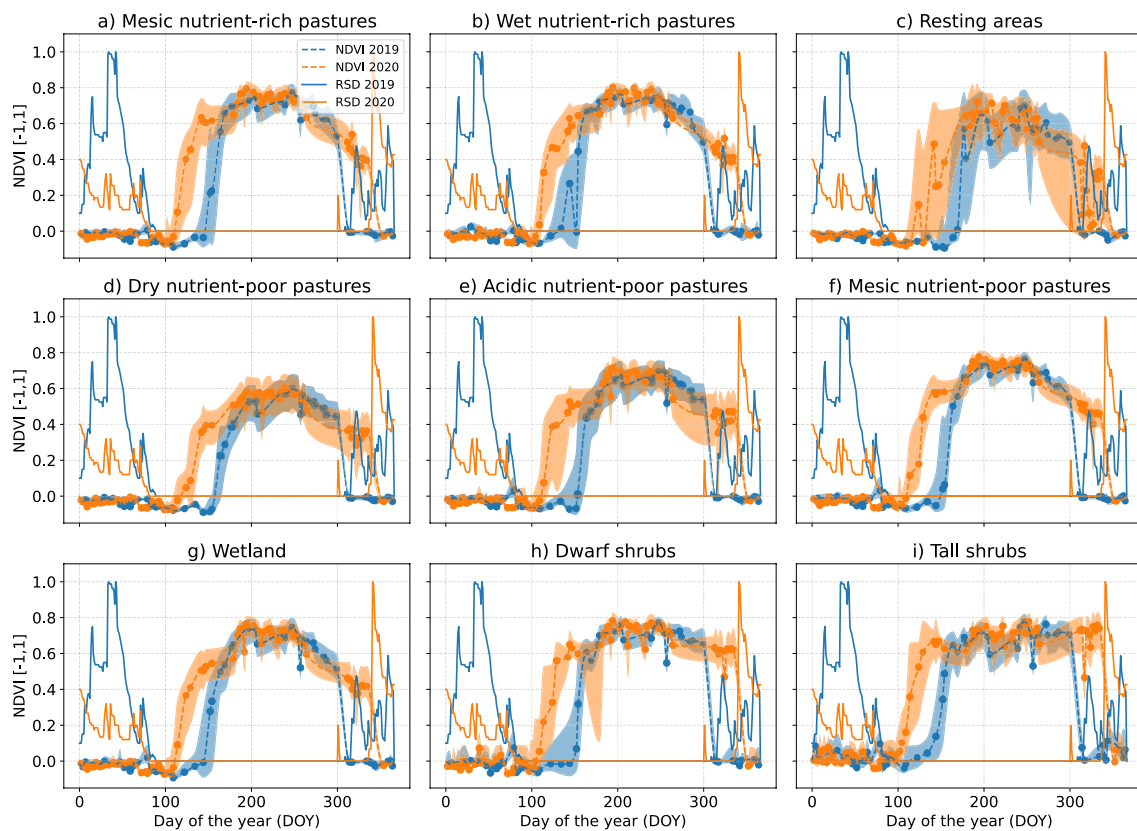
Fig. 3 Example of NDVI (dashed lines and envelopes) and RSD (continuous lines) annual curves in two compared years: 2019 (blue) and 2020 (orange). For NDVI, the variability envelope is delimited by the the 0.25 and 0.75 quantiles of the daily pixel-value distribution, while the dashed line represents the median

intervals of elevation in the range 2000–2800 m. Moreover, the correlation among the indicators and with elevation was investigated. The dependency of the habitat growth upon elevation changes was investigated further by computing the Pearson correlation coefficient *r* between all polygons median AUC and their median elevation (Table 2) in both the first and second season halves. Polygons presenting less than five points in the annual AUC curve were discarded since, after visual inspection, they were found not always representing a realistic growth pattern. Conversely, the descriptors based on the Gompertz function (growth slope and growth maximum) were computed on the annual pixels sets per habitat, leading to more stable curve shapes. The Student test (Student 1908) was computed to check the significance of the estimated correlation coefficients. Following the common practice for this test, correlation coefficients with p-values lower than 0.05 were considered significant.

Results

Annual growth curves

Examples of annual growth curves extracted for every habitat for 2019 and 2020 are shown in Fig. 3. The two years demonstrate clear differences representative of the variations which can be similarly found among other years (supplemental material 1/2). For both 2019 and 2020, the majority of the habitats present annual curves with a relatively low NDVI variability of approximately ± 0.05 around the median (dashed line), as indicated by the 0.25–0.75 quantile envelope. Conversely, resting areas and tall shrubs (Fig. 3c, i) show a larger NDVI variability around ± 0.1. In case of resting areas, covering limited surface (Table 1), this uncertainty is possibly due to data noise or snow-covered pixels not detected in the preprocessing. Mesic, wet pastures, and wetlands (Fig. 3a, b, f, g) reach NDVI 0.8 in full season, while dry pastures (d), acidic ones (e), and resting areas (d) present a lower NDVI plateau. The growth curves of dwarf and tall shrubs (Fig. 3h, i) present a longer plateau with values mainly between 0.6 and 0.8, and a sharper end of season instead of a gradual senescence.

The habitat response to growth disturbances is a key factor for ecosystem productivity (White et al. 2020; Mahaut et al. 2023). Disturbances in mountain rangelands are mainly linked to snow presence variations, being the expression of meteorological variability. This is most strikingly expressed at a seasonal scale with snow persistence at the end of winter. Inter-annual variations in the habitat growth are well represented by the differences between 2019 (Fig. 3 blue) and 2020 (orange) curves. Those primarily regard the season length delimited by the SOG and the EOS (Fig. 2). In particular, the SOG occurs when winter snow disappears, as shown by the RSD time series (Fig. 3 continuous lines).

Similarly the EOS occurs with the beginning snowfall towards the end of the year. For all habitats, the 2019 growth season is shorter since delimited by a more persistent snow in spring (late SOG) and earlier snow arrival in fall (early EOS). This variation does not visibly affect the maximum growth, but rather the area under the curve (AUC), whose variations are analysed in the following section.

Seasonal growth and elevation

The seasonal growth is analysed by means of the NDVI AUC (see "Annual growth curve analysis") for the first
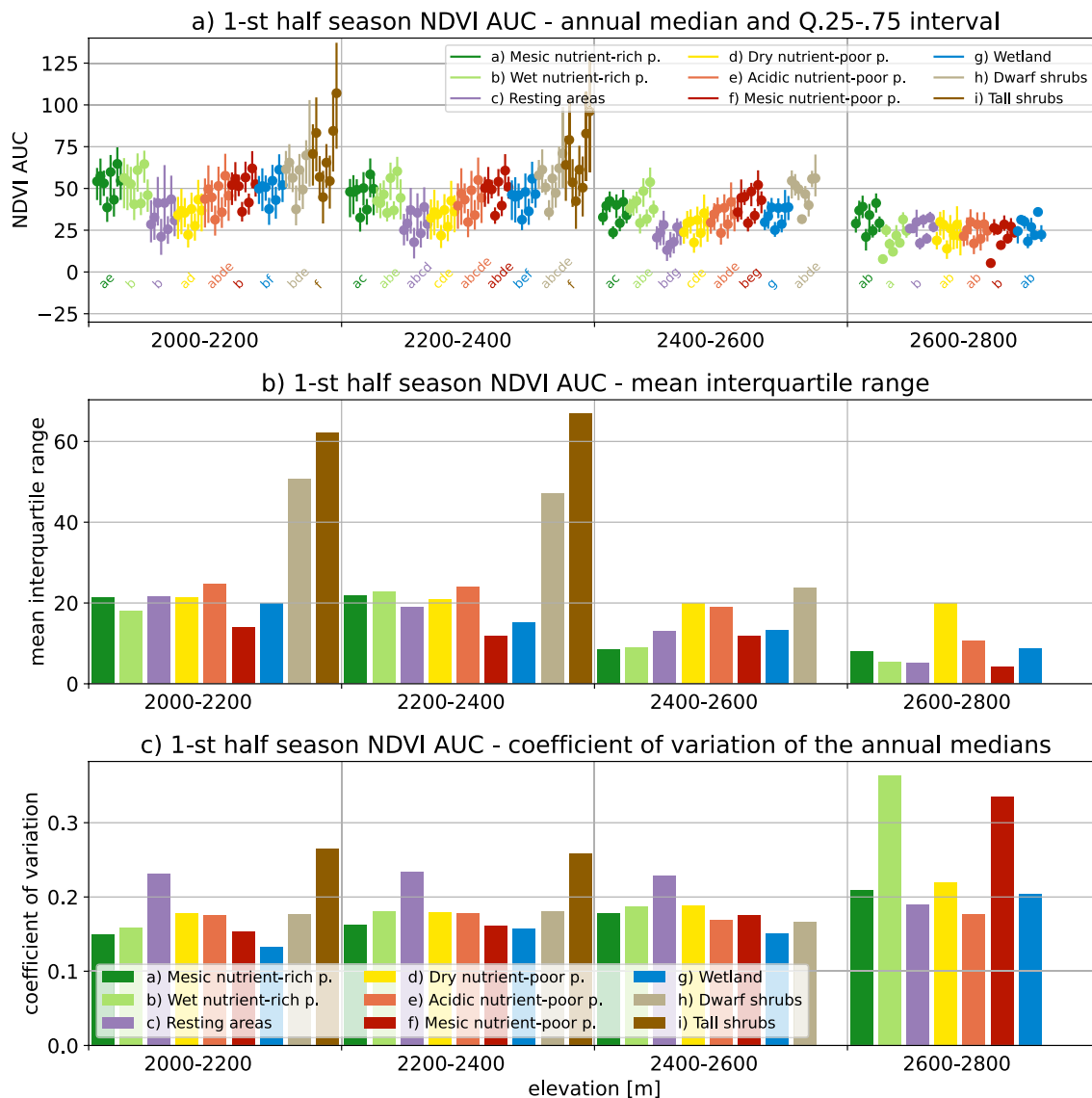
Fig. 4 Plot of the NDVI AUC1 (see "Annual growth curve analysis") for different habitat units (different colors), years (same color bars), and elevation classes (separated by vertical grid lines): **a** annual median (dots) and .25-.75 quantile envelope (error bar) for different years (2016–2023). Letter combinations in the same color of the habitats show statistical similarity according to Tukey's HSD test. **b** Mean interquartile range (equivalent to the mean error bar length in **a**). **c** Coefficient of variation of the annual medians (dots in **a**) for every habitat unit
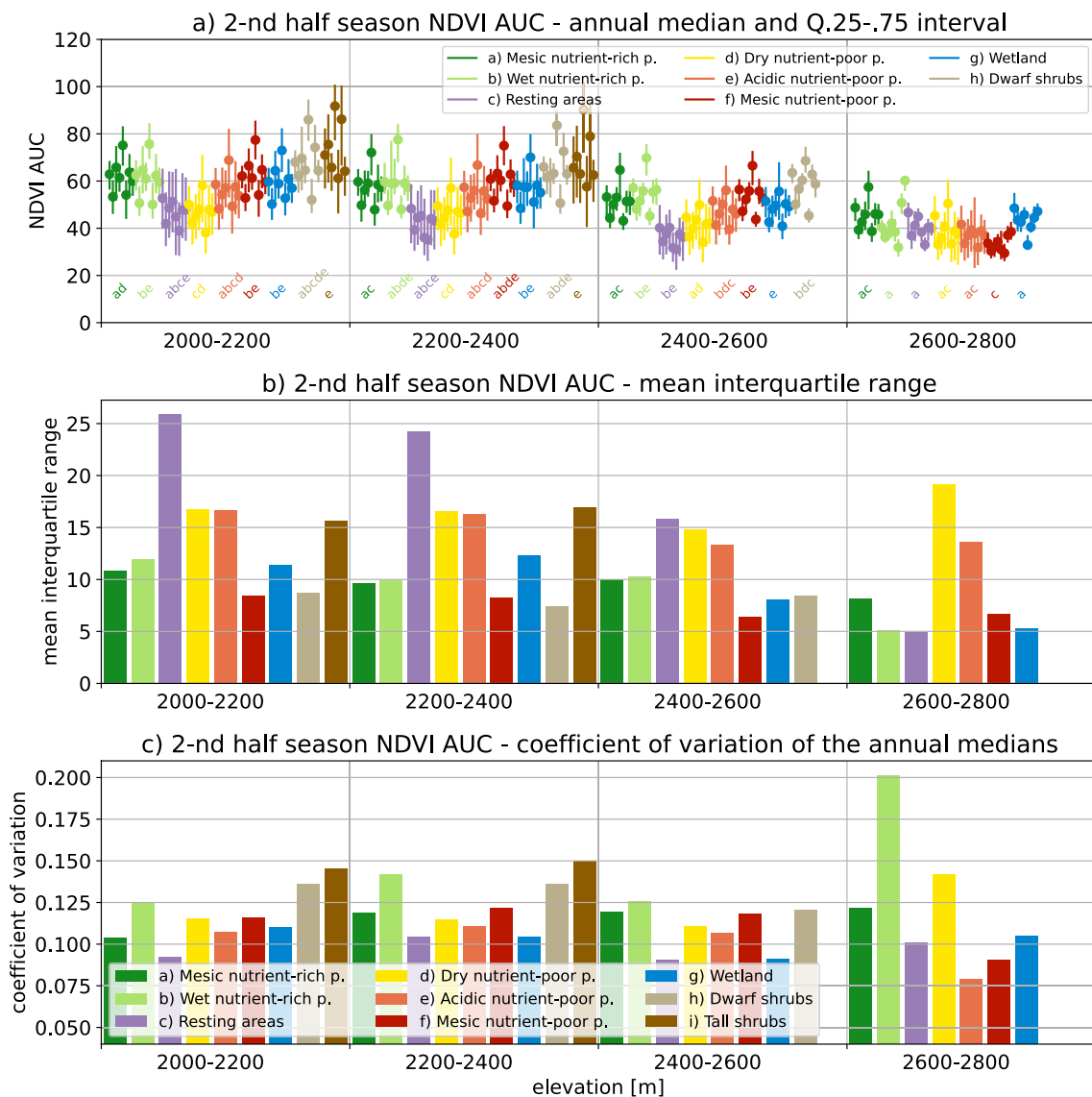
Fig. 5 Plot of the NDVI AUC2 (see "Annual growth curve analysis") for different habitat units (different colors), years (same color bars), and elevation classes (separated by vertical grid lines): **a** Annual median (dots) and .25-.75 quantile envelope (error bar) for different years (2016–2023). Letter combinations in the same color of the habi- tats show statistical similarity according to Tukey's HSD test. **b** Mean interquartile range (equivalent to the mean error bar length in a). **c** Coefficient of variation of the annual medians (dots in a) for every habitat unit

(AUC1) and second (AUC2) halves of the season. These are computed (Figs. 4, 5 panel a) for every habitat (colors), four classes of elevation (separated by vertical grid lines), and the eight available years (2016–2023), represented by adjacent bars of the same color. The statistical variability is represented by the median (dots) and 0.25–0.75 quantiles (error bars) of annual curves. A descending trend in the AUC1 (Fig. 4a) is observed when elevation increases, dropping from the 23–110 range at 2000–2200 m a.s.l., to 5–45 at 2600–2800 m. A similar trend is observed for AUC2 (Fig. 5a). In both season halves and for lower elevation (2000–2200 m), mesic and wet habitats (green shades,

orange, red, and blue colors) present the largest AUC among pastures, mainly in the range 40–80. Conversely, lower AUC values mainly in between 20 and 50 belong to dry pastures (yellow), resting areas (purple), and tall shrubs (brown) pre- sent the lowest values. These differences even out along the elevation profile, until above 2600 m where all units AUC1 mainly vary in 0–40 for the first part of the season and in 30–60 for AUC2. The change in the habitat differences are confirmed by the CLD labels (Figs. 4, 5 panel a), where statistically similar habitats share the same letters.

Tall shrubs (Fig. 4, 5 brown color) keep distinctly higher and variable AUC values with elevation, mainly between 50

and 100, and disappear above 2400 m a.s.l., above the tree-line. Conversely, dwarf shrubs (beige color) present AUC values comparable to wet pastures and persist up to 2600 m of elevation.

The vertical error bars in the panel (a) of Figs. 4 and 5, defined by the AUC of the 0.25–0.75 curves, are based on the variability in daily pixel ensembles. The length of these bars (interquartile range) can be related to the spatial variability of the habitat growth during the year, the spatial variability of snow persistence and land-cover or atmospheric contamination. The means of this quantity (among different years) are displayed again as bars in Figs. 4 and 5 panel b). For the first season half, tall and dwarf shrubs present a sensibly large spatial variability in the growth, with a mean interquartile above 60 and 40, respectively. Conversely, the other habitats vary mainly between 20 and 30. These values tend to diminish sensibly with elevation above 2400 m, partly because pixel data are scarcer and consequently tend to exhibit lower statistical variability. Nevertheless, a similar tendency is confirmed on the same analysis with equal-size random samples of 50 pixels (supplemental material 2/2). For the second half of the season (Fig. 5b), resting areas (purple color) stand out with a mean interquartile range around 25 while the other habitats range between 10 and

17. Similarly to the first season half, these differences reduce above 2400 m of elevation.

The panels c of Figs. 4 and 5 display the coefficient of variation among the AUC median curves of the different years considered (dots in panel a of the same figures). This indicator represents the relative inter-annual variation of the AUC for the different habitats and elevation classes. For the first half season (Fig. 4c) and up to 2600 m, resting areas and tall shrubs present a coefficient of variation higher than 0.2 while all other habitat units mainly lie between 0.1 and 0.2. This pattern changes above 2600 m, where wet nutrient-rich pastures (light green) and mesic nutrient-poor ones (red) present a sensibly higher coefficient of variation above 0.3, while all other units range around 0.2. In the second half of the season (Fig. 5c), the inter-annual coefficient of variation mainly varies between 0.1 and 0.15 for all units with no clear pattern in function of elevation.

The Pearson correlation coefficient r between the AUC for all polygons and their median elevation (Table 2) in both the first and second season halves is in general negative, meaning that all habitats grow less with elevation. Moreover, dry and acidic nutrient-poor pastures present significantly high correlation values for almost all years, on average higher than 0.8 in the first half of the season

Table 2 Pearson correlation coefficient (r) of the median NDVI AUC versus median elevation for different habitat units, computed from every polygon and both the first and second halves of season

Habitat	2016	2017	2018	2019	2020	2021	2022	2023	mean	std
First season half										
Mesic nutrient-rich pastures	− 0.53	− 0.51	− 0.48	− 0.50	− 0.55	− 0.55	− 0.45	− 0.53	− 0.51	0.033
Wet nutrient-rich pastures	− 0.47	− 0.38	− 0.43	− 0.42	− 0.51	− 0.44	− 0.29	− 0.37	− 0.41	0.063
Resting areas	**− 0.74**	**− 0.61**	− 0.59	− 0.58	**− 0.66**	**− 0.65**	− 0.48	**− 0.60**	**− 0.61**	0.070
Dry nutrient-poor pastures	**− 0.82**	**− 0.80**	**− 0.79**	**− 0.87**	**− 0.83**	**− 0.81**	**− 0.77**	**− 0.82**	**− 0.81**	0.027
Acidic nutrient-poor pastures	**− 0.80**	**− 0.78**	**− 0.80**	**− 0.83**	**− 0.81**	**− 0.83**	**− 0.76**	**− 0.80**	**− 0.80**	0.022
Mesic nutrient-poor pastures	− 0.54	− 0.41	− 0.48	− 0.42	− 0.52	− 0.51	− 0.38	− 0.46	− 0.46	0.052
Wetland	− 0.56	− 0.42	− 0.40	− 0.49	− 0.45	− 0.49	− 0.34	− 0.45	− 0.45	0.062
Dwarf shrubs	− 0.27	**− 0.66**	**− 0.67**	**− 0.70**	**− 0.73**	**− 0.66**	**− 0.68**	**− 0.63**	**− 0.62**	0.136
Tall shrubs	− 0.26	− 0.02	− 0.17	− 0.14	− 0.19	− 0.30	0.02	0.12	− 0.11	0.135
Second season half										
Mesic nutrient-rich pastures	− 0.36	− 0.57	− 0.20	− 0.39	− 0.28	− 0.38	− 0.38	− 0.53	− 0.38	0.113
Wet nutrient-rich pastures	− 0.30	− 0.48	0.04	− 0.32	− 0.18	− 0.26	− 0.10	− 0.36	− 0.24	0.153
Resting areas	− 0.47	**− 0.67**	− 0.34	− 0.52	− 0.47	− 0.47	− 0.36	**− 0.67**	− 0.49	0.115
Dry nutrient-poor pastures	− 0.57	**− 0.75**	**− 0.64**	− 0.56	**− 0.73**	− 0.57	**− 0.71**	− 0.58	**− 0.63**	0.073
Acidic nutrient-poor pastures	**− 0.69**	**− 0.75**	**− 0.70**	**− 0.70**	**− 0.75**	**− 0.76**	**− 0.74**	**− 0.76**	**− 0.73**	0.028
Mesic nutrient-poor pastures	− 0.33	− 0.55	− 0.15	− 0.57	− 0.16	− 0.35	− 0.26	**− 0.64**	− 0.37	0.177
Wetland	− 0.34	− 0.36	− 0.12	− 0.31	− 0.15	− 0.35	− 0.29	− 0.40	− 0.29	0.093
Dwarf shrubs	− 0.44	− 0.39	− 0.07	− 0.20	− 0.44	− 0.27	− 0.54	− 0.37	− 0.33	0.141
Tall shrubs	0.03	− 0.33	− 0.13	− 0.10	0.07	0.05	− 0.02	− 0.44	− 0.10	0.173

The mean (mean) and standard deviation (std) columns refer to the annual correlation values on the left. Strong correlation values, higher than 0.6 or lower than −0.6, are marked in bold

and higher than 0.7 in the second half, and with a low standard deviation among the years (Table 2 mean and std columns). Therefore, the growth of these habitats appears to be strongly related to the elevation profile. Conversely, resting areas and dwarf shrubs growth present a weaker (0.5–0.65) correlation, suggesting a weak dependency on elevation changes. For these two habitats the correlation estimation is also uncertain and varying through the years also because it is based on 40–70 data points, while for the previously mentioned habitats it is based on 120–220 data points.

Growth dynamics

The statistical descriptors of the growth curves, described in "Annual growth curve analysis", are put in relation by computing the Pearson correlation coefficient (Table 3). Among the tested combinations of descriptors, $r_{g,s}$ (SOG vs growth slope) is significantly high and positive for all pasture units and resting areas, meaning that a later SOG (higher value) is associated to a higher growth slope. Both quantities are anticorrelated to ACU1, decreasing when

the SOG and slope increase, as shown by the negative coefficients $r_{g,a1}$ and $r_{s,a1}$. Moreover, all pasture habitats show a significant positive correlation between AUC2 and EOS ($r_{a2,e}$).

The growth curves of the wetland habitat present a weaker but similar correlation pattern as the other pastures. Conversely, dwarf and tall shrubs only show the AUC2 correlated to the EOS ($r_{a2,e}$), with a stronger value of 0.9 for dwarf shrubs and a weaker one of 0.73 for tall shrubs.

Discussion

Methodological considerations

In the present paper, a satellite-based time series analysis on mountain grassland ecosystem was developed to investigate the variability of annual growth in different pasture and shrub habitats at different elevation. This land surface phenology investigation was based on the satellite images from the Sentinel-2 mission, which constitute the current

Table 3 Correlation coefficients r_{xy}, where x and y are growth curve descriptors ("Annual growth curve analysis"), namely: SOG (g), growth slope (s), AUC1 ($a1$), AUC2 ($a2$), EOS (e), curve maximum (m)

Habitat	$r_{g,s}$	$r_{g,a1}$	$r_{g,m}$	$r_{g,a2}$	$r_{g,e}$	$r_{s,a1}$	$r_{s,m}$	$r_{s,a2}$
Mesic nutrient-rich p	**0.85**	**−0.93**	0.09	−0.14	−0.22	−0.71	−0.16	0.29
Wet nutrient-rich p	**0.93**	**−0.82**	−0.01	−0.33	−0.40	**−0.76**	−0.07	−0.18
Resting areas	**0.82**	**−0.92**	−0.31	−0.50	−0.61	−0.69	−0.39	−0.17
Dry nutrient-poor p	**0.90**	**−0.89**	−0.29	−0.20	−0.40	**−0.75**	−0.49	−0.02
Acidic nutrient-poor p	**0.83**	**−0.92**	0.07	−0.16	−0.41	**−0.75**	−0.33	0.15
Mesic nutrient-poor p	**0.85**	**−0.93**	0.20	−0.23	−0.33	**−0.79**	−0.13	0.21
Wetland	**0.74**	**−0.85**	0.19	0.03	−0.13	−0.41	−0.18	0.61
Dwarf shrubs	0.10	−0.16	−0.37	0.28	0.51	−0.70	−0.48	−0.03
Tall shrubs	−0.02	−0.24	−0.30	0.41	0.06	0.07	−0.65	0.06

Habitat	$r_{s,e}$	$r_{a1,m}$	$r_{a1,a2}$	$r_{a1,e}$	$r_{m,a2}$	$r_{m,e}$	$r_{a2,e}$
Mesic nutrient-rich p	0.24	0.08	0.34	0.40	−0.10	−0.30	**0.92**
Wet nutrient-rich p	−0.24	0.09	0.57	0.69	0.14	−0.20	**0.90**
Resting areas	−0.27	0.46	0.35	0.50	0.23	0.17	**0.87**
Dry nutrient-poor p	−0.08	0.52	0.30	0.49	−0.04	−0.18	**0.90**
Acidic nutrient-poor p	−0.05	0.07	0.30	0.54	−0.20	−0.43	**0.87**
Mesic nutrient-poor p	0.14	0.02	0.37	0.45	−0.02	−0.24	**0.93**
Wetland	0.51	−0.07	0.32	0.45	−0.31	−0.54	**0.91**
Dwarf shrubs	−0.01	0.09	0.33	0.32	−0.06	−0.09	**0.90**
Tall shrubs	0.53	0.23	0.07	0.11	−0.26	−0.54	**0.73**

Bold values indicate significant correlation coefficients (p-value < 0.05)

freely available state-of-the-art product with an optimal balance among spatial resolution, sensor quality, temporal coverage, and revisit time. Data acquisition based on EOdal allowed systematic access to the entire image time-series for a large ROI.

Moreover, the use of a data dictionary for the NDVI pixel preprocessing and analysis allowed dealing with multiple pixel attributes in a much more agile way than considering whole image cubes. In summary, the main data-filtering steps which allowed minimizing data contamination are the exclusion of: images presenting more than 30% cloud coverage, all pixels classified as cloudy or non vegetated using the Sentinel-2 Scene Classification Layer, the pixels north-facing, and pixels in shadow (see Appendix A, Appendix B, and "Annual growth curve analysis" for more details). This allowed approaching a stable reflectance signal from the pixel set belonging to a single habitat, showing a statistical variability imputable to different growth conditions and species variability along the elevation profile.

For the considered region, Sentinel-2 delivers complete annual time series since 2016. This time span offers a rather variable snow persistence for the study region, depending on winter precipitation and temperatures. The snowpack melt date, measured at the Scuol station (see "Ancillary variables"), varies between the beginning of April (2017) and the end of May (2021). While these data represent well the variability of land surface phenology, multiple decades of images are necessary to investigate the effect of climate trends. Future research in this direction could employ images from the Landsat program (NASA) to extend the investigation to a larger time coverage. The lower spatio-temporal resolution of these images with respect to Sentinel-2 can be improved by means of data fusion techniques (see e.g. Oriani et al. 2021; Hu et al. 2024), allowing the estimation of fine-resolution heterogeneity by stochastic generation. As additional possible improvement, periodical updates of the habitat survey map can provide a more precise mapping of the vegetation spatial distribution, reducing data noise in the growth curves.

Finally, NDVI should be considered informative mainly of the growth pattern and should not be used alone to estimate absolute growth, which is linked to different physiological traits of species (Kattenborn et al. 2019). In particular, NDVI saturates at high values, which affects the representation of maximum growth in the annual curves especially in dense vegetation (Li et al. 2013). Empirical correction methods have been developed (e.g. Gu et al. 2013) without being general and showing variable performance in wet and dry habitats (Lu et al. 2015; Tang et al. 2017). The growth curve integral (AUC) is affected by saturation to a minor extent (Yan et al. 2022) and remains valuable in comparative and spatial analysis as done in the present study.

Two types of pasture growth dynamics

With the present analysis, we identified two main types of growth patterns, belonging to dry and wet pastures respectively. This difference, as explained in the following, is linked to the vegetation response to snow persistence and elevation changes.

The AUC statistics (Figs. 4, 5) show that mesic and wet pasture habitats present a larger cumulative growth and less variable in space compared to dry pastures and resting areas during the whole growth season at elevations from 2000 to 2400 m a.s.l. At higher elevation, we observed a generalized reduction of these differences. As suggested by plot studies along elevation transects (Dongdong et al. 2020; Mainetti et al. 2023), this homogenization of pasture growth among habitats can be explained by compositional variations of species due to water scarcity and lower temperature conditions, usually found at mountain tops. In these conditions, more productive and wet habitats may approach a species composition more similar to dry ones, with a related reduction of productivity.

Dependence of growth on elevation

The polygon-wise analysis of the AUC in relation to elevation (Table 2) reveals a significant correlation between growth and elevation in dry and less productive pasture habitats. These habitats are highly dependent on hydroclimatic (thermal lapse and soil humidity rates) (Pape and Löffler 2017; Mainetti et al. 2023) and soil chemistry variations (Güsewell et al. 2012) along the elevation profile. Growth in the first half of the season appears to be consistently more dependent on elevation with respect to growth in the second half. Conversely, wetter habitats, more frequently present along valley axes, are influenced more strongly by the valley orientation and morphology, determining orographic precipitation regimes, wind exposure, and affecting soil type and thickness (Swanson et al. 1988).

Impact of inter-annual weather variability on growth

Following past research (White et al. 2020; Mahaut et al. 2023), the relation between ecosystem stability and productivity can be investigated with indicators of i) variability and ii) response rate to disturbance events. Indicators of variability (i), representing the sensitivity of the habitats to seasonal weather variations, are present in this study examining both growth variability in space (Figs. 4, 5 panel b) and time (Figs. 4, 5 panel c). Moreover, the average response rate (ii) to seasonal snow persistence, is examined with the growth curve of the habitats (Fig. 3) and put in relation to productivity (correlation coefficients in Table 3).

Inter-annual snow persistence variations turn out to be important for growth in pasture habitats, with growth curve AUC variations of 15–20 %, as shown by the inter-annual coefficient of variation of the AUC, more pronounced in the first part of the season (Figs. 4, 5 panel c). There is no strong difference of this variation depending on the vegetation type, with only resting areas tending to be moderately more vulnerable than the other habitats.

The statistical descriptors of the growth curves (Table 3) allow analyzing the growth dynamics of the vegetation in the mountain rangeland ecosystem. Pastures habitats with delayed start of the growth season, controlled by snow persistence, show an increase of the growth slope (r_{gs}). This suggests a compensation in the growth process by increased growth speed after late snow melt. These dynamics can be explained by mechanisms of damping snow persistence variations. While similar results have been previously observed in plot-scale studies in alpine meadow and tundra ecosystems (Billings and Bliss 1959; Choler 2005; Jonas et al. 2008) or belowground processes (Choler 2018) and undersnow growth (Tieszen et al. 1978; Fetcher and Shaver 1990; Walker et al. 1994; Parker et al. 2022), we can confirm these findings on a landscape scale. Moreover, the presented method allows to estimate the relationships across multiple habitats and elevations with comparably low effort. Consequently, the interactions of growth dynamics in these habitats can be monitored throughout space and time, allowing to trace if, where and how climate variability—and in the long run climate change—affect mountain habitats the most.

Nevertheless, both the SOG and the growth slope are negatively correlated with the AUC in the first part of the season ($r_{g,a1}$ and $r_{s,a1}$), suggesting that the mentioned compensation mechanism, faster growth after late-melting snow, does not fully recover the lack of assimilation due to a shorter season. Therefore, in agreement to previous investigations (Choler 2015; Xie et al. 2017), snow persistence still appear as one main controlling factor on the first half of the growth season amplitude and productivity. Similarly, autumn snow occurrence ends the season and limits growth in pastures, as suggested by the correlation between the AUC2 and EOS $r_{a2,e}$, with the EOS being linked to the first snow occurrence (see Fig. 2). Also, growth in the second season half appears to be rather independent from the first half (low $r_{a1,a2}$).

It should be noted that grazing can also influence standing biomass, which potentially influences the temporal pattern of growth. Nevertheless, land management for the study area follows a stable pattern in space, with only minor variations in time in response to seasonal weather conditions. Therefore, the growth pattern is still mainly affected by climate variability.

Shrub habitats: a matter of tallness

The two analyzed shrub habitats show different AUC statistics (Figs. 4, 5 beige and brown colors). Although being present in our ROI only up to 2400 m, tall shrubs present the highest growth curve values among all habitats with no big variations in the AUC in function of elevation. Since tall vegetation does not cope well with low air temperature and wind-driven heat loss (Wilson 1959; Holtmeier and Broll 2010; Ives and Barry 2019; Körner 2021), thermal excursion may be the main limiting factor for their growth at high elevation. Conversely, dwarf shrubs present lower growth values comparable to pasture habitats and moderately correlated with elevation changes (Table 2).

Both shrub types vary twice more their growth in space than pastures in the first half of the season (Figs. 4 panel b) and tall ones show substantial inter-annual variations in the AUC, 15 and 25% among 2016–2023 AUC1 and ACU2 medians (Figs. 4, 5 panel c).

While, with both shrub types, there isn't a significant correlation between cumulative growth and the variation of the SOG, the arrival of snow in autumn (EOS) seems to limit more importantly their growth ($r_{a2,e}$ in Table 3).

Conclusions and future perspectives

In this paper, we presented a high-resolution satellite image analysis focused on the characterization of nine habitat types in mountain rangelands. The study is based on the satellite product Sentinel-2 and the habitat map of the mountain pastures surrounding the Swiss National Park (Grisons canton, Switzerland). An image-analysis workflow was developed to derive the growth pattern of the small-scale habitat in a complex topographic setting. Based on the spectral index NDVI, the workflow allowed to investigate the habitat phenology in relation with elevation and snow persistence.

The main findings of this study are that wet and dry pastures exhibit two main different growth patterns: the former more productive at mid elevation, the latter growing more variably in space and more sensitive to elevation. The difference in growth progressively attenuate at high elevation above 2400 m a.s.l., suggesting a similar productivity of the habitats.

Also, the correlation study among the growth-curve descriptors suggests the presence, at a regional scale, of some dynamics previously observed at the plot scale: snow melt, controlling the beginning of the growing season, appears as the main limiting factor for the cumulative growth of all pasture habitats. This delay is partially compensated by a quicker growth in years with late snow melt. Similarly, the arrival of snow in autumn limits accumulation in the second part of the season. These dynamics at the end of the season

also affects dwarf shrubs, while tall shrubs grow variably in space and independently of elevation until the treeline. For all habitats, inter-annual weather fluctuations impact growth importantly, with 15–20% of AUC variation, with repercussions on the annual rangeland productivity.

These findings, in continuity with previous plot-scale studies, expand the knowledge of habitat seasonality and their response to changes in hydro-climate factors, in particular snow persistence. Moreover, the presented regional analysis suggests the importance of continuous and possibly real-time monitoring of vegetation growth in mountain rangelands for management purposes.

Possible advancements of this research include the comparison of the findings from on-site plot analysis and growth models, with further application to other mountain areas. This study characterized different habitat types by means of statistical descriptors of the growth curve. These descriptors can be computed pixel-wise to obtain raster maps as supporting tools for rangeland management. For example, these maps can be used to detect annual anomalies in pasture productivity to optimize animal carrying capacity and provide more targeted and flexible support schemes for farmers. Moreover, the data can be used to monitor the spread of invasive shrub species over the pasture lands due to land abandonment. Another possible application is the continuous real-time monitoring of the beginning and end of season in different pasture areas to improve grazing management, especially for remote high-elevation areas.

The maps can also be the object of an in-depth investigation of climate and topographic factors influencing seasonal productivity. This last type of analysis requires the realization of detailed annual weather maps and topographic descriptors, representative of the complex space variations present in the alpine setting.

Appendix A. Data acquisition workflow for Sentinel-2 images

The workflow developed for the programmatic retrieval of the Sentinel-2 images consists in the following steps:

1. According to the parameters set for the EOdal mapper, the Sentinel-2 data catalog is queried for a given time span and ROI with the STAC protocol https://stacspec.org. A series of sub-queries to divide the image time series in data chunks.
2. For every data chunk, the sub-query is sent to the server and the images are downloaded.
3. Within the EOdal preprocessing module, all image pixels classified as any cloud type or non-vegetation cover are masked. this is done according to the Sentinel-2

Scene Classification Layer (SCL), available as raster band for every image. In this case, snow pixels were not masked since they include mixed-spectrum values allowing to better observe the early growth of vegetation.
4. All bands in every image are linearly interpolated on a defined target grid of 10 m resolution (in line with Sentinel-2 resolution) covering the ROI in the Swiss local CRS CH1903/LV95 (EPSG:2056). This leads to a 4D data cube for every data chunk, whose dimensions consists in xy image coordinates, number of bands, and different temporal frames.
5. For every data cube, the NDVI images are computed using Sentinel-2 red (B04) and near-infrared (B08) bands with the standard formula NDVI = (B08-B04)/(B08+B04). This leads to a 3D NDVI cube consisting in xy image coordinates and temporal frame.
6. Every data cube is stored locally.

Appendix B. Preprocessing workflow for the NDVI images

The obtained NDVI images are preprocessed as follows. First, the pasture classification map ("Study region and data") of the ROI is interpolated on the same xy grid of the NDVI cube, using the nearest-neighbor interpolation. The same is done for the DEM ("Ancillary variables") using the bi-linear interpolation. These two raster variables are then used in the following steps, run iteratively on every NDVI data cube ("Acquisition of the satellite images"):

1. The NDVI cube is loaded in python.
2. Using the rasterized habitat map, images are discarded if they contain less than 10% pixels informed among the ones mapped as habitat units. This allows avoiding too biased point values in the extracted annual growth curves. Among the discarded images there are also the ones presenting extensive snow cover for all units, corresponding to days following summer snow events. Those are easily detected since they correspond to isolated negative peaks in the summer period common for all NDVI growth curves.
3. For every accepted image, the shadow cast by mountains is computed using the package python-dem-shadow (adapted script in the Code Availability section) based on the DEM and the solar angle available as metadata for every Sentinel-2 scene. This way, every pixel is labeled as covered by shadow or not.
4. From the DEM, the aspect of every pixel was derived using the python package richdem (https://pypi.org/project/richdem/). The aspect is used exclude from the analy-

sis non south-ward pixels (see "Annual growth curve analysis").

5. Pixels mapped as habitat units are extracted from every image and stored in a python dictionary, where every item represents an attribute linked to pixels and contains a vector of values, one for each pixel.

More information on the dataset structure is available in the documentation of the attached code ("Conclusions").

Appendix C. The Gompertz growth function

The Gompertz model (Gompertz 1825) is a sigmoidal type of curve suitable to represent growth processes. Similarly, we use here the following equation:

$$y = -ae^{-e^{c(x-b)}} + d \tag{1}$$

with y being the fitted NDVI value, x the DOY, a the curve amplitude parameter, b the x coordinate of the sigmoid flex point, c the growth slope factor, and d the y coordinate of the maximum growth plateau. The function was fitted with a least-square method on the Pchip interpolation of the data, since it preserves a more stable fitting in case of scarce NDVI data in the year. The following parameter boundaries were imposed to preserve a realistic shape of the NDVI growth curve: [0, 2] for a, with 0 for zero curve amplitude (no growth) and 2 for the maximum NDVI theoretical amplitude from -1 to 1, [50, 200] for b, limiting the center of the growth slope between DOY 50 and 200, [0, 1] for c, with 0 for horizontal slope and 1 for vertical slope, and [0, 1] for d, with 0 for the curve maximum equal to zero (no growth) and 1 for the maximum equal to 1 (NDVI theoretical maximum).

Declarations

References

Alves Aguiar D, Adami M, Fernando Silva W, Friedrich Theodor Rudorff B, Pupin Mello M, Dos Santos Vila Da Silva J (2010) Modis time series to assess pasture land. In: 2010 IEEE international geoscience and remote sensing symposium. IEEE, Honolulu, pp 2123–2126. https://doi.org/10.1109/IGARSS.2010.5649388

Amies AC, Dymond JR, Shepherd JD, Pairman D, Hoogendoorn C, Sabetizade M, Belliss SE (2021) National mapping of New Zealand pasture productivity using temporal Sentinel-2 data. Remote Sens 13:1481. https://doi.org/10.3390/rs13081481

Asrar G, Fuchs M, Kanemasu ET, Hatfield JL (1984) Estimating absorbed photosynthetic radiation and leaf area index from spectral reflectance in wheat. Agron J 76:300–306. https://doi.org/10.2134/agronj1984.00021962007600020029x

Bayle A, Carlson BZ, Thierion V, Isenmann M, Choler P (2019) Improved mapping of mountain shrublands using the Sentinel-2 red-edge band. Remote Sens 11:2807. https://doi.org/10.3390/rs11232807. number: 23 Publisher: Multidisciplinary Digital Publishing Institute

Becker A, Körner C, Brun JJ, Guisan A, Tappeiner U (2007) Ecological and land use studies along elevational gradients. Mt Res Dev 27:58–65. https://doi.org/10.1659/0276-4741(2007)27[58:EALUSA]2.0.CO;2

Bella D, Faivre R, Ruget F, Seguin B, Guérif M, Combal B, Weiss M, Rebella C (2004) Remote sensing capabilities to estimate pasture production in France. Int J Remote Sens 25:5359–5372. https://doi.org/10.1080/01431160410001719849

Billings WD, Bliss LC (1959) An alpine snowbank environment and its effects on vegetation, plant development, and productivity. Ecology 40:388–397. https://doi.org/10.2307/1929755

Boschetti M, Bocchi S, Brivio PA (2007) Assessment of pasture production in the Italian Alps using spectrometric and remote sensing information. Agric Ecosyst Environ 118:267–272. https://doi.org/10.1016/j.agee.2006.05.024

Braunisch V, Patthey P, Arlettaz R (2016) Where to combat shrub encroachment in alpine timberline ecosystems: combining remotely-sensed vegetation information with species habitat modelling. PLoS ONE 11:e0164318. https://doi.org/10.1371/journal.pone.0164318

Choler P (2005) Consistent shifts in alpine plant traits along a meso-topographical gradient. Arct Antarct Alp Res 37:444–453. https://doi.org/10.1657/1523-0430(2005)037[0444:CSIAPT]2.0.CO;2

Choler P (2015) Growth response of temperate mountain grasslands to inter-annual variations in snow cover duration. Biogeosciences 12:3885–3897. https://doi.org/10.5194/bg-12-3885-2015

Choler P (2018) Winter soil temperature dependence of alpine plant distribution: implications for anticipating vegetation changes under a warming climate. Perspect Plant Ecol Evol Syst 30:6–15. https://doi.org/10.1016/j.ppees.2017.11.002

Cocca G, Sturaro E, Gallo L, Ramanzin M (2012) Is the abandonment of traditional livestock farming systems the main driver of mountain landscape change in alpine areas? Land Use Policy 29:878–886. https://doi.org/10.1016/j.landusepol.2012.01.005

Colpaert A, Kumpula J, Nieminen M (2003) Reindeer pasture biomass assessment using satellite remote sensing. ARCTIC 56:147–158. https://doi.org/10.14430/arctic610

Crepaz H, Niedrist G, Wessely J, Rossi M, Dullinger S (2021) Resident vegetation modifies climate-driven elevational shift of a mountain sedge. Alp Bot 131:13–25. https://doi.org/10.1007/s00035-020-00243-6

Deroche B, Pradel P, Baumont R (2020) Long-term evolution and prediction of feed value for permanent mountain grassland hay: analysis of a 32-year data set in relation to climate change. Grass Forage Sci 75:18–27. https://doi.org/10.1111/gfs.12465

Dietl W, Berger P, Ofner M (1981) Die Kartierung des Pflanzenstandortes und der futterbaulichen Nutzungseignung von Naturwiesen. Eidg. Forschungsanstalt für landwirtschaftlichen Pflanzenbau und Arbeitsgemeinschaft zur Förderung des Futterbaues, Zürich-Reckenholz, Switzerland

Dirnböck T, Dullinger S, Grabherr G (2003) A regional impact assessment of climate and land?use change on alpine vegetation. J Biogeogr 30:401–417. https://doi.org/10.1046/j.1365-2699.2003.00839.x

Dongdong C, Qi L, Zhe L, Fuquan H, Xin C, Shixiao X, Xinquan Z, Liang Z (2020) Variations of forage yield and nutrients with altitude gradients and their influencing factors in alpine meadow of Sanjiangyuan, China. J Soil Sci Plant Nutr 20:2164–2174. https://doi.org/10.1007/s42729-020-00284-0

Du Q, Sun Y, Guan Q, Pan N, Wang Q, Ma Y, Li H, Liang L (2022) Vulnerability of grassland ecosystems to climate change in the Qilian mountains, Northwest China. J Hydrol 612:128305. https://doi.org/10.1016/j.jhydrol.2022.128305

Engler R, Randin CF, Thuiller W, Dullinger S, Zimmermann NE, Araújo MB, Pearman PB, Le Lay G, Piedallu C, Albert CH, Choler P, Coldea G, De Lamo X, Dirnböck T, Gégout JC, Gómez-García D, Grytnes JA, Heegaard E, Høistad F, Noguès-Bravo D, Normand S, Puşcaş M, Sebastiá MT, Stanisci A, Theurillat JP, Trivedi MR, Vittoz P, Guisan A (2011) 21st century climate change threatens mountain flora unequally across Europe: climate change impacts on mountain florae. Glob Change Biol 17:2330–2341. https://doi.org/10.1111/j.1365-2486.2010.02393.x

Ernakovich JG, Hopping KA, Berdanier AB, Simpson RT, Kachergis EJ, Steltzer H, Wallenstein MD (2014) Predicted responses of arctic and alpine ecosystems to altered seasonality under climate change. Glob Change Biol 20:3256–3269. https://doi.org/10.1111/gcb.12568

Feng Y, Wu J, Zhang J, Zhang X, Song C (2017) Identifying the relative contributions of climate and grazing to both direction and magnitude of alpine grassland productivity dynamics from 1993 to 2011 on the northern Tibetan Plateau. Remote Sens 9:136. https://doi.org/10.3390/rs9020136

Fetcher N, Shaver GR (1990) Environmental sensitivity of ecotypes as a potential influence on primary productivity. Am Nat 136:126–131. https://doi.org/10.1086/285085

Filippa G, Cremonese E, Galvagno M, Isabellon M, Bayle A, Choler P, Carlson BZ, Gabellani S, Morra di Cella U, Migliavacca M (2019) Climatic drivers of greening trends in the Alps. Remote Sens 11:2527. https://doi.org/10.3390/rs11212527. number: 21 Publisher: Multidisciplinary Digital Publishing Institute

Filippa G, Cremonese E, Galvagno M, Bayle A, Choler P, Bassignana M, Piccot A, Poggio L, Oddi L, Gascoin S, Costafreda-Aumedes S, Argenti G, Dibari C (2022) On the distribution and productivity of mountain grasslands in the Gran Paradiso National Park, NW Italy: a remote sensing approach. Int J Appl Earth Observ Geoinf 108:102718. https://doi.org/10.1016/j.jag.2022.102718

Fisher J, Mustard J, Vadeboncoeur M (2006) Green leaf phenology at Landsat resolution: scaling from the field to the satellite. Remote Sens Environ 100:265–279. https://doi.org/10.1016/j.rse.2005.10.022

Frei ER, Ghazoul J, Matter P, Heggli M, Pluess AR (2014) Plant population differentiation and climate change: responses of grassland species along an elevational gradient. Glob Change Biol 20:441–455. https://doi.org/10.1111/gcb.12403

Fritsch FN, Butland J (1984) A method for constructing local monotone piecewise cubic interpolants. SIAM J Sci Stat Comput 5:300–304. https://doi.org/10.1137/0905021. publisher: Society for Industrial and Applied Mathematics

Gompertz B (1825) XXIV. On the nature of the function expressive of the law of human mortality, and on a new mode of determining the value of life contingencies. In a letter to Francis Baily, Esq. F. R. S. & c. Philos Trans Roy Soc Lond 115:513–583. https://doi.org/10.1098/rstl.1825.0026

Grabherr G, Gottfried M, Pauli H (2010) Climate change impacts in alpine environments. Geogr Compass 4:1133–1153. https://doi.org/10.1111/j.1749-8198.2010.00356.x

Graf LV, Perich G, Aasen H (2022) Eodal: an open-source python package for large-scale agroecological research using earth observation and gridded environmental data. Comput Electron Agric 203:107487. https://doi.org/10.1016/j.compag.2022.107487

Gu Y, Wylie BK, Howard DM, Phuyal KP, Ji L (2013) NDVI saturation adjustment: a new approach for improving cropland performance estimates in the Greater Platte River Basin, USA. Ecol Indic 30:1–6. https://doi.org/10.1016/j.ecolind.2013.01.041

Guerini Filho M, Kuplich TM, Quadros FLFD (2020) Estimating natural grassland biomass by vegetation indices using Sentinel 2 remote sensing data. Int J Remote Sens 41:2861–2876. https://doi.org/10.1080/01431161.2019.1697004

Güsewell S, Peter M, Birrer S (2012) Altitude modifies species richness-nutrient indicator value relationships in a country-wide survey of grassland vegetation. Ecol Indic 20:134–142. https://doi.org/10.1016/j.ecolind.2012.02.011

Hanna MM, Steyn-Ross DA, Steyn-Ross M (1999) Estimating biomass for New Zealand pasture using optical remote sensing techniques. Geocarto Int 14:89–94. https://doi.org/10.1080/10106049908542121

Hoersch B, Braun G, Schmidt U (2002) Relation between landform and vegetation in alpine regions of Wallis, Switzerland. A multiscale remote sensing and GIS approach. Comput Environ Urban Syst 26:113–139. https://doi.org/10.1016/S0198-9715(01)00039-4

Hogrefe K, Patil V, Ruthrauff D, Meixell B, Budde M, Hupp J, Ward D (2017) Normalized difference vegetation index as an estimator for abundance and quality of avian herbivore forage in Arctic Alaska. Remote Sens 9:1234. https://doi.org/10.3390/rs9121234

Holtmeier FK, Broll G (2010) Wind as an ecological agent at treelines in North America, the Alps, and the European Subarctic. Phys Geogr 31:203–233. https://doi.org/10.2747/0272-3646.31.3.203

Hu G, Jiang Y, Li S, Xiong L, Tang G, Mariethoz G (2024) Super-resolution of digital elevation models by using multiple-point statistics and training image selection. Comput Geosci 191:105688. https://doi.org/10.1016/j.cageo.2024.105688

Huber N, Ginzler C, Pazur R, Descombes P, Baltensweiler A, Ecker K, Meier E, Price B (2023) Countrywide classification of permanent

grassland habitats at high spatial resolution. Remote Sens Ecol Conserv 9:133–151. https://doi.org/10.1002/rse2.298

Huete A, Justice C, Liu H (1994) Development of vegetation and soil indices for MODIS-EOS. Remote Sens Environ 49:224–234. https://doi.org/10.1016/0034-4257(94)90018-3

Inouye DW (2020) Effects of climate change on alpine plants and their pollinators. Ann NY Acad Sci 1469:26–37. https://doi.org/10.1111/nyas.14104

Ives JD, Barry RG (2019) Arctic and alpine environments. Routledge. Google-Books-ID: pfS2DwAAQBAJ

Jin Y, Yang X, Qiu J, Li J, Gao T, Wu Q, Zhao F, Ma H, Yu H, Xu B (2014) Remote sensing-based biomass estimation and its spatio-temporal variations in temperate grassland, Northern China. Remote Sens 6:1496–1513. https://doi.org/10.3390/rs6021496

Jonas T, Rixen C, Sturm M, Stoeckli V (2008) How alpine plant growth is linked to snow cover and climate variability. J Geophys Res Biogeosci. https://doi.org/10.1029/2007JG000680

Kattenborn T, Fassnacht FE, Schmidtlein S (2019) Differentiating plant functional types using reflectance: which traits make the difference? Remote Sens Ecol Conserv 5:5–19. https://doi.org/10.1002/rse2.86

Körner C (2021) The cold range limit of trees. Trends Ecol Evol 36:979–989. https://doi.org/10.1016/j.tree.2021.06.011

Lal JB, Gulati AK, Bist MS (1991) Satellite mapping of alpine pastures in the Himalayas. Int J Remote Sens 12:435–443. https://doi.org/10.1080/01431169108929664

Lass LW, Prather TS, Glenn NF, Weber KT, Mundt JT, Pettingill J (2005) A review of remote sensing of invasive weeds and example of the early detection of spotted knapweed (*Centaurea maculosa*) and babysbreath (*Gypsophila paniculata*) with a hyperspectral sensor. Weed Sci 53:242–251. https://doi.org/10.1614/WS-04-044R2

Li Z, Huffman T, McConkey B, Townley-Smith L (2013) Monitoring and modeling spatial and temporal patterns of grassland dynamics using time-series MODIS NDVI with climate and stocking data. Remote Sens Environ 138:232–244. https://doi.org/10.1016/j.rse.2013.07.020

Li H, Li FY, Guo J, Gao X (2023) An improved dynamic threshold method for determining the start of the vegetation greening season in remote sensing monitoring: the case of Inner Mongolia. Ecol Inform 78:102378. https://doi.org/10.1016/j.ecoinf.2023.102378

Liu H, Mi Z, Lin L, Wang Y, Zhang Z, Zhang F, Wang H, Liu L, Zhu B, Cao G, Zhao X, Sanders NJ, Classen AT, Reich PB, He JS (2018) Shifting plant species composition in response to climate change stabilizes grassland primary production. Proc Natl Acad Sci 115:4051–4056. https://doi.org/10.1073/pnas.1700299114

Lu L, Kuenzer C, Wang C, Guo H, Li Q (2015) Evaluation of three MODIS-derived vegetation index time series for dryland vegetation dynamics monitoring. Remote Sens 7:7597–7614. https://doi.org/10.3390/rs70607597

Ma Y, He T, McVicar TR, Liang S, Liu T, Peng W, Song DX, Tian F (2024) Quantifying how topography impacts vegetation indices at various spatial and temporal scales. Remote Sens Environ 312:114311. https://doi.org/10.1016/j.rse.2024.114311

MacDonald D, Crabtree J, Wiesinger G, Dax T, Stamou N, Fleury P, Gutierrez Lazpita J, Gibon A (2000) Agricultural abandonment in mountain areas of Europe: environmental consequences and policy response. J Environ Manag 59:47–69. https://doi.org/10.1006/jema.1999.0335

Mahaut L, Choler P, Denelle P, Garnier E, Thuiller W, Kattge J, Lemauviel-Lavenant S, Lavorel S, Munoz F, Renard D, Serra-Diaz JM, Viovy N, Violle C (2023) Trade-offs and synergies between ecosystem productivity and stability in temperate grasslands. Glob Ecol Biogeogr 32:561–572. https://doi.org/10.1111/geb.13645

Mainetti A, Ravetto Enri S, Pittarello M, Lombardi G, Lonati M (2023) Main ecological and environmental factors affecting forage yield and quality in alpine summer pastures (NW-Italy Gran Paradiso National Park). Grass Forage Sci 78:254–267. https://doi.org/10.1111/gfs.12609

Matsushita B, Yang W, Chen J, Onda Y, Qiu G (2007) Sensitivity of the enhanced vegetation index (EVI) and normalized difference vegetation index (NDVI) to topographic effects: a case study in high-density Cypress Forest. Sensors 7:2636–2651. https://doi.org/10.3390/s7112636

Mayer R, Kaufmann R, Vorhauser K, Erschbamer B (2009) Effects of grazing exclusion on species composition in high-altitude grasslands of the Central Alps. Basic Appl Ecol 10:447–455. https://doi.org/10.1016/j.baae.2008.10.004

Noroozi J, Körner C (2018) A bioclimatic characterization of high elevation habitats in the Alborz mountains of Iran. Alp Bot 128:1–11. https://doi.org/10.1007/s00035-018-0202-9

Oriani F, McCabe MF, Mariethoz G (2021) Downscaling multispectral satellite images without colocated high-resolution data: a stochastic approach based on training images. IEEE Trans Geosci Remote Sens 59:3209–3225. https://doi.org/10.1109/TGRS.2020.3008015

Pape R, Löffler J (2017) Determinants of arctic-alpine pasture resources: the need for a spatially and functionally fine-scaled perspective. Geogr Ann Ser B 99:353–370. https://doi.org/10.1080/04353676.2017.1368833

Parker TC, Unger SL, Moody ML, Tang J, Fetcher N (2022) Intraspecific variation in phenology offers resilience to climate change for *Eriophorum vaginatum*. Arct Sci 8:935–951. https://doi.org/10.1139/as-2020-0039

Peng F, Xue X, Xu M, You Q, Jian G, Ma S (2017) Warming-induced shift towards forbs and grasses and its relation to the carbon sequestration in an alpine meadow. Environ Res Lett 12:044010. https://doi.org/10.1088/1748-9326/aa6508

Piepho HP (2004) An algorithm for a letter-based representation of all-pairwise comparisons. J Comput Graph Stat 13:456–466. https://doi.org/10.1198/1061860043515

Pullanagari R, Kereszturi G, Yule I (2018) Integrating airborne hyperspectral, topographic, and soil data for estimating pasture quality using recursive feature elimination with random forest regression. Remote Sens 10:1117. https://doi.org/10.3390/rs10071117

Raab C, Riesch F, Tonn B, Barrett B, Meißner M, Balkenhol N, Isselstein J (2020) Target-oriented habitat and wildlife management: estimating forage quantity and quality of semi-natural grasslands with Sentinel-1 and Sentinel-2 data. Remote Sens Ecol Conserv 6:381–398. https://doi.org/10.1002/rse2.149

Schneider MK, Law R, Illian JB (2006) Quantification of neighbourhood-dependent plant growth by Bayesian hierarchical modelling. J Ecol 94:310–321. https://doi.org/10.1111/j.1365-2745.2005.01079.x

Schöb C, Kammer PM, Kikvidze Z, Choler P, Veit H (2008) Changes in species composition in alpine snowbeds with climate change inferred from small-scale spatial patterns. Web Ecol 8:142–159. https://doi.org/10.5194/we-8-142-2008

Schwörer C, Colombaroli D, Kaltenrieder P, Rey F, Tinner W (2015) Early human impact (5000–3000 BC) affects mountain forest dynamics in the Alps. J Ecol 103:281–295. https://doi.org/10.1111/1365-2745.12354

Serrano J, Shahidian S, Marques Da Silva J (2018) Monitoring seasonal pasture quality degradation in the Mediterranean Montado ecosystem: proximal versus remote sensing. Water 10:1422. https://doi.org/10.3390/w10101422

Shang R, Liu R, Xu M, Liu Y, Zuo L, Ge Q (2017) The relationship between threshold-based and inflexion-based approaches for extraction of land surface phenology. Remote Sens Environ 199:167–170. https://doi.org/10.1016/j.rse.2017.07.020

Spiegelberger T, Matthies D, Müller-Schärer H, Schaffner U (2006) Scale-dependent effects of land use on plant species richness of mountain grassland in the European Alps. Ecography 29:541–548. https://doi.org/10.1111/j.0906-7590.2006.04631.x

Student (1908) Probable error of a correlation coefficient. Biometrika 6:302–310. https://doi.org/10.1093/biomet/6.2-3.302

Stumpf F, Schneider MK, Keller A, Mayr A, Rentschler T, Meuli RG, Schaepman M, Liebisch F (2020) Spatial monitoring of grassland management using multi-temporal satellite imagery. Ecol Indic 113:106201. https://doi.org/10.1016/j.ecolind.2020.106201

Swanson FJ, Kratz TK, Caine N, Woodmansee RG (1988) Landform effects on ecosystem patterns and processes. Bioscience 38:92–98. https://doi.org/10.2307/1310614

Tang L, Dong S, Sherman R, Liu S, Liu Q, Wang X, Su X, Zhang Y, Li Y, Wu Y, Zhao H, Zhao C, Wu X (2015) Changes in vegetation composition and plant diversity with rangeland degradation in the alpine region of Qinghai-Tibet Plateau. Rangel J 37:107. https://doi.org/10.1071/RJ14077

Tang X, Ma M, Ding Z, Xu X, Yao L, Huang X, Gu Q, Song L (2017) Remotely monitoring ecosystem water use efficiency of grassland and cropland in China's arid and semi-arid regions with MODIS data. Remote Sens 9:616. https://doi.org/10.3390/rs9060616

Tang Y, Chen R, Xie J, Ma D, Wang C, Wang C, Xie Q, Yin G (2023) Spatiotemporal variations of leaf senescence velocity on the Tibetan Plateau grasslands. Ecol Indic 156:111094. https://doi.org/10.1016/j.ecolind.2023.111094

Taylor B, Dini P, Kidson J (1985) Determination of seasonal and inter-annual variation in New Zealand pasture growth from NOAA-7 data. Remote Sens Environ 18:177–192. https://doi.org/10.1016/0034-4257(85)90047-1

Tieszen LL, Billings WD, Golley F, Lange OL, Olson JS (Eds) (1978) Vegetation and production ecology of an Alaskan arctic tundra. Volume 29 of ecological studies. Springer New York, New York. https://doi.org/10.1007/978-1-4612-6307-4

Tukey JW (1949) Comparing individual means in the analysis of variance. Biometrics 5:99. https://doi.org/10.2307/3001913

Wachendorf M, Fricke T, Möckel T (2018) Remote sensing as a tool to assess botanical composition, structure, quantity and quality of temperate grasslands. Grass Forage Sci 73:1–14. https://doi.org/10.1111/gfs.12312

Walker MD, Webber PJ, Arnold EH, Ebert-May D (1994) Effects of interannual climate variation on aboveground phytomass in alpine vegetation. Ecology 75:393–408. https://doi.org/10.2307/1939543

Wang S, Dai E, Jia L, Wang Y, Huang A, Liao L, Cai L, Fan D (2023) Assessment of multiple factors and interactions affecting grassland degradation on the Tibetan Plateau. Ecol Indic 154:110509. https://doi.org/10.1016/j.ecolind.2023.110509

Weber D, Schaepman-Strub G, Ecker K (2018) Predicting habitat quality of protected dry grasslands using Landsat NDVI phenology. Ecol Indic 91:447–460. https://doi.org/10.1016/j.ecolind.2018.03.081

Weber D, Schwieder M, Ritter L, Koch T, Psomas A, Huber N, Ginzler C, Boch S (2023) Grassland-use intensity maps for Switzerland based on satellite time series: challenges and opportunities for ecological applications. Remote Sens Ecol Conserv. https://doi.org/10.1002/rse2.372

Wehn S, Lundemo S, Holten JI (2014) Alpine vegetation along multiple environmental gradients and possible consequences of climate change. Alp Bot 124:155–164. https://doi.org/10.1007/s00035-014-0136-9

White HJ, Gaul W, Sadykova D, León-Sánchez L, Caplat P, Emmerson MC (2020) Quantifying large-scale ecosystem stability with remote sensing data. Remote Sens Ecol Conserv 6:354–365. https://doi.org/10.1002/rse2.148

Wilson JW (1959) Notes on wind and its effects in Arctic-alpine vegetation. J Ecol 47:415–427. https://doi.org/10.2307/2257374

Xie J, Kneubühler M, Garonna I, Notarnicola C, De Gregorio L, De Jong R, Chimani B, Schaepman ME (2017) Altitude-dependent influence of snow cover on alpine land surface phenology. J Geophys Res Biogeosci 122:1107–1122. https://doi.org/10.1002/2016JG003728

Yan J, Zhang G, Ling H, Han F (2022) Comparison of time-integrated NDVI and annual maximum NDVI for assessing grassland dynamics. Ecol Indic 136:108611. https://doi.org/10.1016/j.ecolind.2022.108611

Zhou Y, Zhang L, Xiao J, Chen S, Kato T, Zhou G (2014) A comparison of satellite-derived vegetation indices for approximating gross primary productivity of grasslands. Rangel Ecol Manag 67:9–18. https://doi.org/10.2111/REM-D-13-00059.1

Zhu X, Li Q, Guo C (2024) Evaluation of the monitoring capability of various vegetation indices and mainstream satellite band settings for grassland drought. Ecol Inform 82:102717. https://doi.org/10.1016/j.ecoinf.2024.102717